Supporting Information for "Flat slab-induced hydration weakening and destruction of the North China Craton"

Jyotirmoy Paul, Arne Spang, Andrea Piccolo

Bayerisches Geoinstitut, Universität Bayreuth, 95447 Bayreuth, Germany

Contents of this file

1. Text S1
2. Tables S1 to S2
3. Figures S1 to S3

Text S1. Thermomechanical Code

The thermomechanical finite differences code LaMEM (Kaus et al., 2016) solves for the conservation of momentum, mass and energy (eq. 1-3), using a staggered grid in combination with a marker-in-cell approach (Harlow & Welch, 1965).

$$\frac{\partial \tau_{ij}}{\partial x_j} - \frac{\partial P}{\partial x_i} + \rho g_i = 0 \tag{1}$$

$$\frac{\partial v_i}{\partial x_i} = 0 \tag{2}$$

$$\rho C_p \frac{DT}{Dt} = \frac{\partial}{\partial x_i}\left(k\frac{\partial T}{\partial x_i}\right) + H \tag{3}$$

τ_{ij} is the Cauchy stress deviator, $x_i (i = 1, 2, 3)$ denotes the Cartesian coordinates, P is pressure (positive in compression), ρ density, g_i gravitational acceleration, v_i the velocity vector, C_p the specific heat capacity, T the temperature, k the thermal conductivity, H the volumetric heat source and D/Dt is the material time derivative. Free slip conditions are applied to the boundaries of the model domain, allowing movement parallel to the domain edges while setting perpendicular velocities to 0 (with the exception of the oceanic plate inflow on the right boundary). At the top of the setup, we include sticky air above the stabilized free surface (Duretz et al., 2011; Kaus et al., 2010). The rocks are characterized by a temperature- and strain rate-dependent visco-elasto-plastic rheology where the strain rate is the sum of the elastic, viscous and plastic components:

$$\dot{\varepsilon}_{ij} = \dot{\varepsilon}_{ij}^{\mathrm{el}} + \dot{\varepsilon}_{ij}^{\mathrm{vi}} + \dot{\varepsilon}_{ij}^{\mathrm{pl}} \tag{4}$$

$\dot{\varepsilon}_{ij}$ denotes the total deviatoric strain rate tensor, while $\dot{\varepsilon}_{ij}^{\mathrm{el}}$, $\dot{\varepsilon}_{ij}^{\mathrm{vi}}$ and $\dot{\varepsilon}_{ij}^{\mathrm{pl}}$ represent the elastic, viscous and plastic strain rate components. A detailed discussion of this equation and all of its components is given by (Kaus et al., 2016), but here we will focus on the material parameters which impact the three components.

The elastic component $\dot{\varepsilon}_{ij}^{\mathrm{el}}$ is inverse proportional to the shear modulus G:

$$\dot{\varepsilon}_{ij}^{\mathrm{el}} = \frac{1}{2G}\frac{D\tau_{ij}}{Dt}, \tag{5}$$

where $D\tau_{ij}/Dt$ corresponds to the objective derivative of the stress tensor. For simplicity, we chose $G = 60$ GPa for all materials.

The viscous strain rate component $\dot{\varepsilon}_{ij}^{\mathrm{vi}}$ is subdivided into diffusion and dislocation creep (eq. 6):

$$\dot{\varepsilon}_{ij}^{\mathrm{vi}} = \dot{\varepsilon}_{ij}^{\mathrm{dif}} + \dot{\varepsilon}_{ij}^{\mathrm{dis}} = \frac{\tau_{ij}}{2}\left(\frac{1}{\eta_{\mathrm{dif}}} + \frac{1}{\eta_{\mathrm{dis}}}\right), \tag{6}$$

where η_{dif} and η_{dis} are defined as follows:

$$\eta_{\mathrm{dif}} = \frac{1}{2}(B_{\mathrm{dif}})^{-1}\mathrm{exp}\left(\frac{E_{\mathrm{dif}}}{RT}\right), \tag{7}$$

$$\eta_{\mathrm{dis}} = \frac{1}{2}(B_{\mathrm{dis}})^{-\frac{1}{n}}(\dot{\varepsilon}_{II}^{\mathrm{dis}})^{\frac{1}{n}-1}\mathrm{exp}\left(\frac{E_{\mathrm{dis}}}{nRT}\right), \tag{8}$$

where B is the creep constant, E the activation energy, $\dot{\varepsilon}_{II}^{\mathrm{dis}}$ the square root of the second invariant of the dislocation creep strain rate ($\dot{\varepsilon}_{II}^{\mathrm{dis}} = (\frac{1}{2}\dot{\varepsilon}_{ij}^{\mathrm{dis}}\dot{\varepsilon}_{ij}^{\mathrm{dis}})^{1/2}$), n the powerlaw exponent, R the universal gas constant and T the temperature.

The plastic component is characterized by the Drucker-Prager failure criterion (Drucker & Prager, 1952) which is a good approximation of Byerlee's law (Byerlee, 1978):

$$\tau_{II} \leq \sin(\phi)P + \cos(\phi)c_0 \tag{9}$$

τ_{II} is the square root of the second invariant of the stress tensor ($\tau_{II} = (\frac{1}{2}\tau_{ij}\tau_{ij})^{1/2}$), ϕ is the friction angle, P the pressure and c_0 the cohesion. Equation 9 describes how much stress can be accommodated with visco-elastic deformation.

In addition to the described rheology, we also employ lower and upper cut-offs to the effective viscosity of 10^{18} Pa s and 10^{25} Pa s respectively. The partitioning between the different rheological components cannot be solved analytically but requires local iterations in each node of the grid.

Table S1: List of Rheological parameters

unit	thickness (km)	reference density kg m^{-3}	prefactor (diff)	activation energy (diff) kJ/mol	activation volume (diff)	prefactor (disl)	activation energy (disl) kJ/mol	activation volume (disl)	n	Reference
Continental crust	0-40	2700	-	-	-	1.25×10^{-9}	123	0	3.2	(Tirel et al., 2008)
Upper mantle	100-660	3300	1.5×10^{9}	375	5×10^{-6}	1.1×10^{5}	530	8.5×10^{-6}	3.5	(Hirth & Kohlstedt, 2003)
Lower mantle	660-1000	3400	1.5×10^{9}	375	5×10^{-6}	1.1×10^{5}	530	8.5×10^{-6}	3.5	”
Continental lithosphere	40-100	2900	1.5×10^{9}	375	5×10^{-6}	1.1×10^{5}	530	15×10^{-6}	3.5	”
Cratonic lithosphere	100-200	3200 - 3400	1.5×10^{9}	375	9.5×10^{-6}	1.1×10^{5}	530	1.5×10^{-6}	10^{6}	”
Weak cratonic lithosphere	100-200	3200 - 3400	10^{6}	440	4×10^{-6}	90	260	11×10^{-6}	3.5	”
Slab	-	3300	1.5×10^{9}	375	9.5×10^{-6}	1.1×10^{5}	530	15×10^{-6}	3.5	”
Dense lower crust	30-70	3400-3550	10^{6}	335	4×10^{-6}	90	520	22×10^{-6}	3.5	”
Weak MLD	60-100	3300	10^{6}	440	4×10^{-6}	90	260	11×10^{-6}	3.5	”

Friction angle (ϕ) and cohesion (c_0) for all models are 30° and 10^{6} Pa

Table S2: List of model parameters

Model	Hydration weakening	Weakening rate	Weak MLD	Dense lower crust	Reference craton density (ρ_i^0, kg m^{-3})	Destruction% after 100 Myr
M1	Yes	R1	No	No	3400	87
M2	Yes	R1	No	No	3300	66
M3	Yes	R1	No	No	3200	7
M4	Yes	R2	No	No	3400	87
M5	Yes	R2	No	No	3300	70
M6	Yes	R2	No	No	3200	7
M7	Yes	R3	No	No	3400	86
M8	Yes	R3	No	No	3300	47
M9	Yes	R3	No	No	3200	6
M10	No	-	No	No	3400	10
M11	No	-	No	No	3300	5
M12	No	-	No	No	3200	1
M13	No	-	No	Yes	3400	8
M14	No	-	No	Yes	3300	11
M15	No	-	No	Yes	3200	8
M16	No	-	Yes	No	3400	37
M17	No	-	Yes	No	3300	0
M18	No	-	Yes	No	3200	0

Additional Supporting Information (Files uploaded separately)

1. Captions for Movies S1

Movie S1. Animation showing the destruction of the NCC from model M2. Descriptions of different colors are given in Fig. 2.

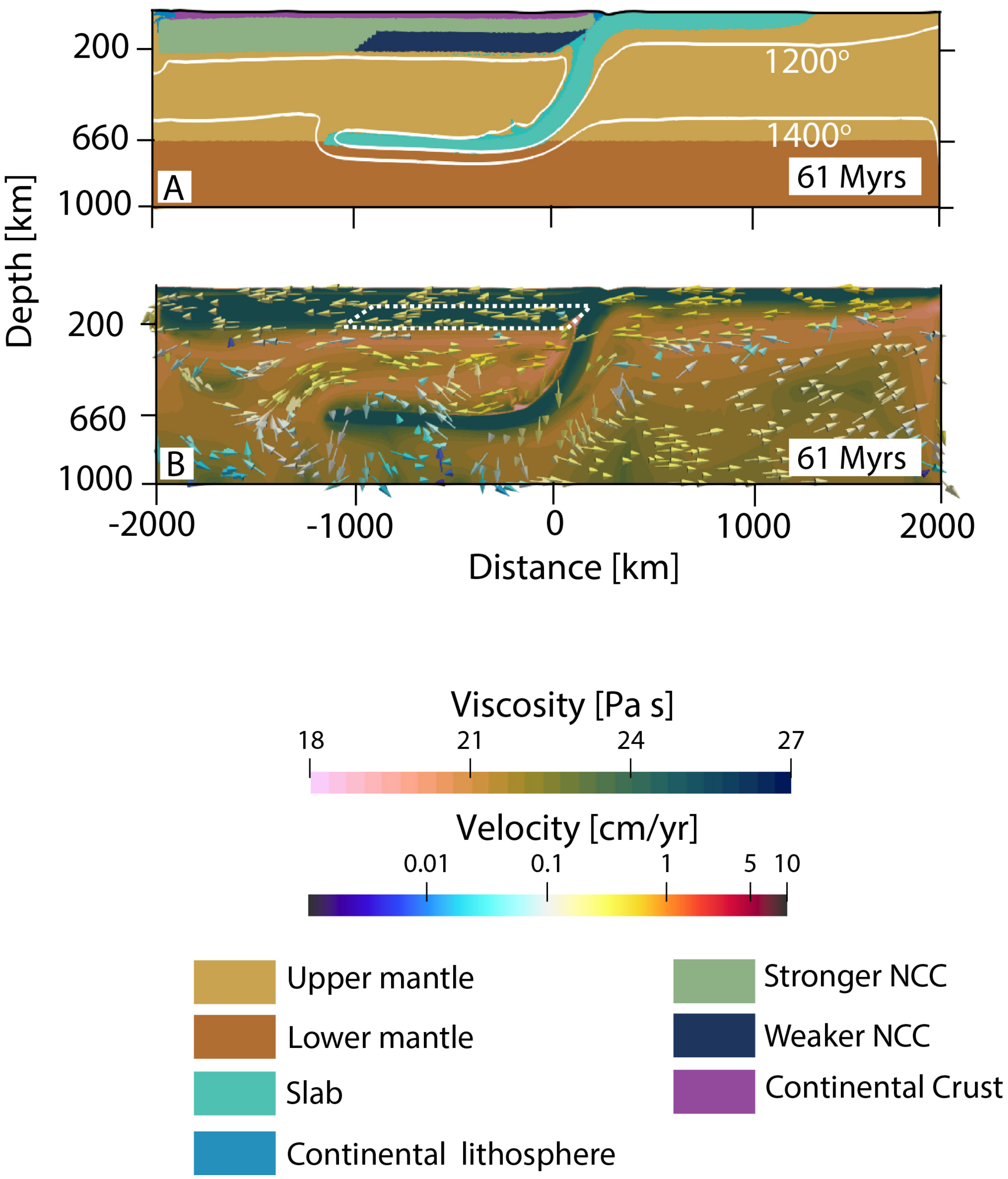

Figure S1. Snapshot of the NCC evolution from model M10 at 61 Myr. Background colors in A represent geological unit/phases which are indexed below. Dark blue region indicates the weak craton which is forming lithospheric drips. Solid white lines indicate isotherms of 1200 °C and 1400 °C. Background colors in B represent viscosity and the arrows represent mantle flow velocity. Viscosity and velocity scales are given below. White dashed line represents the craton, which is not destroyed in this model.

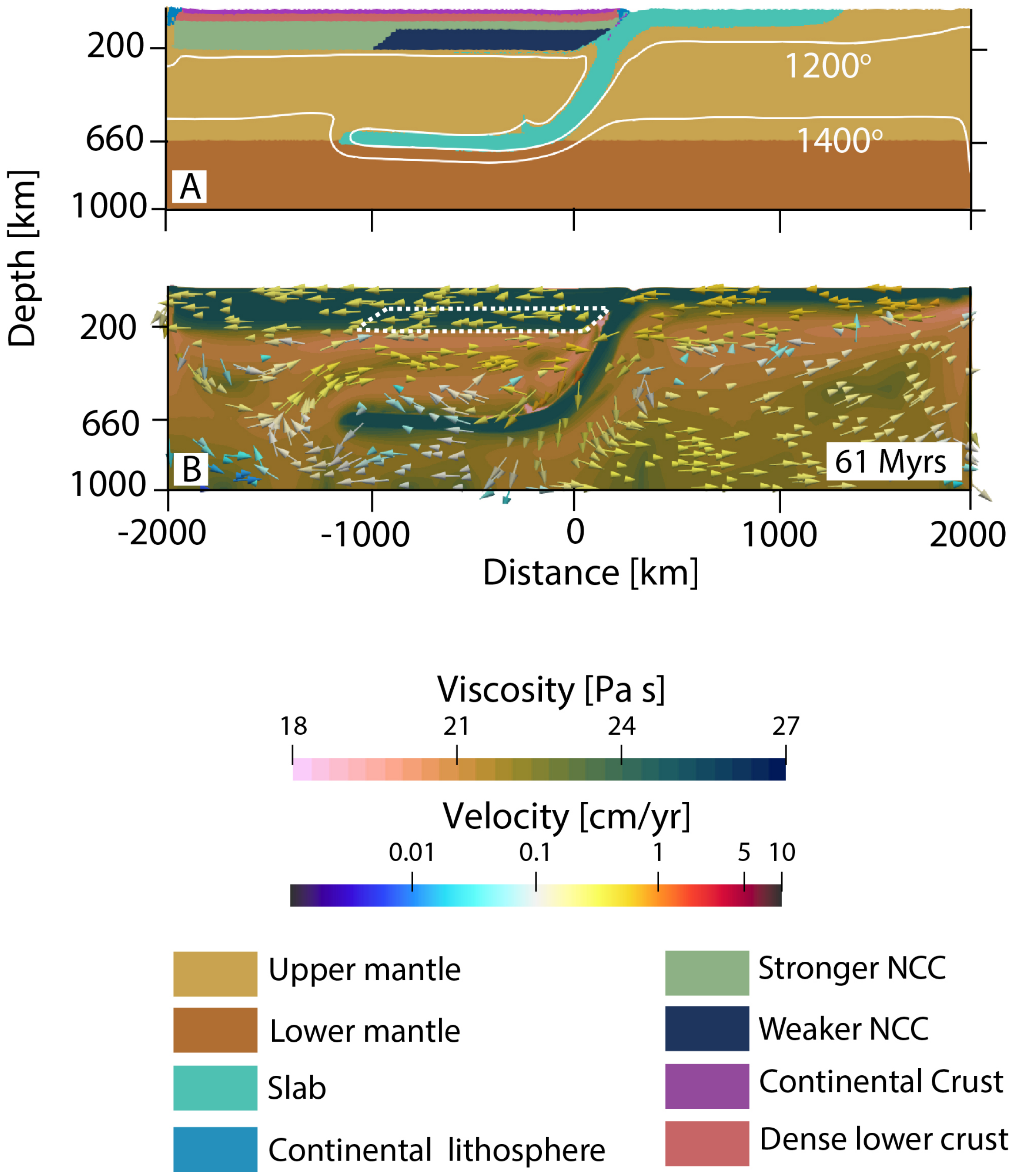

Figure S2. Snapshot of the NCC evolution in presence of a dense lower crust (pink colored region in A, model 13) at 61 Myr. Figure description is exactly same as the Fig. S1. No craton destruction observed in this model.

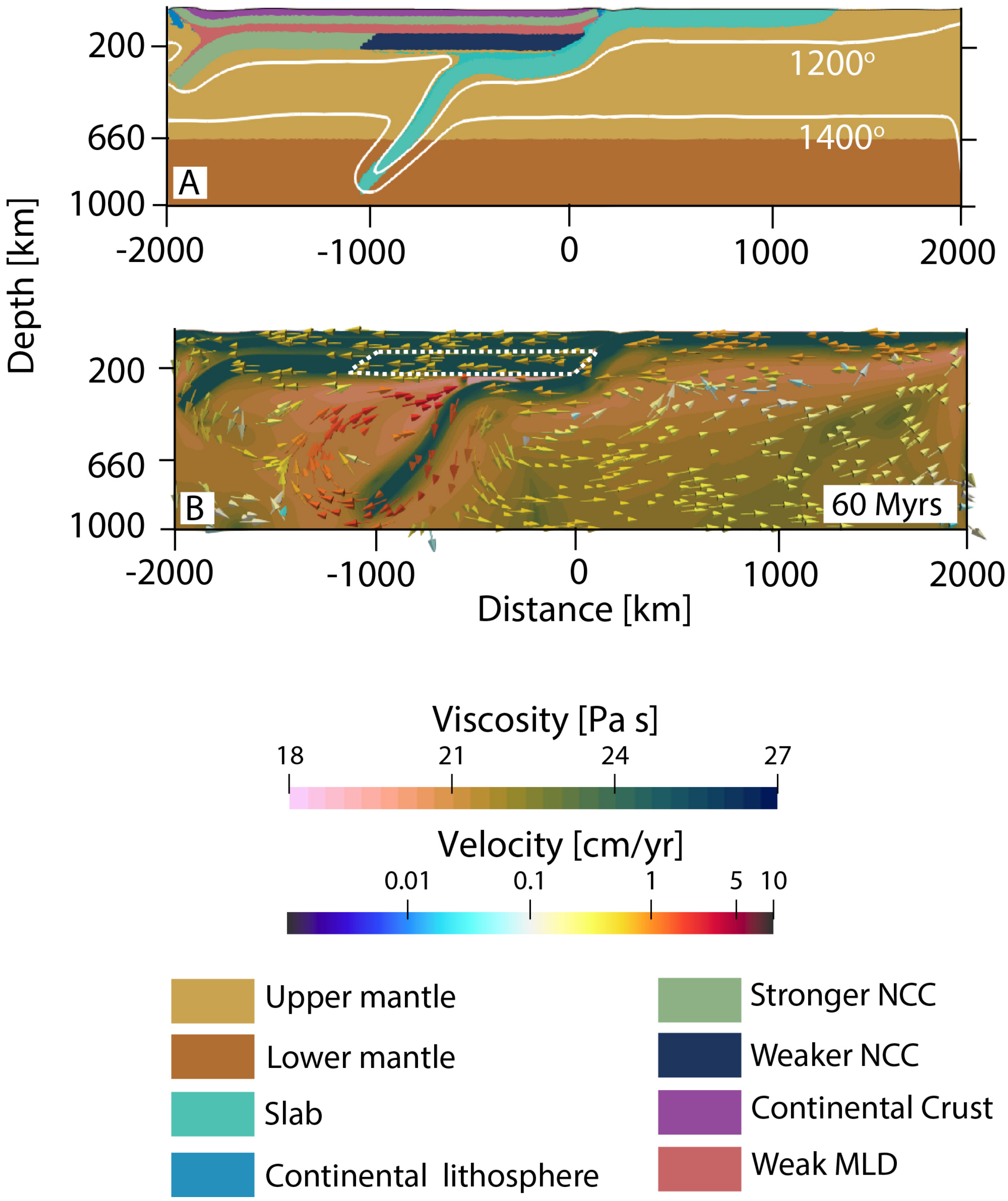

Figure S3. Snapshot of the NCC evolution in presence of a weak MLD (pink colored region in A, model 16) at 60 Myr. Figure description is exactly same as the Fig. S1. The craton starts delaminating from the western margin.

References

Byerlee, J. (1978). Friction of rocks. In *Rock friction and earthquake prediction* (pp. 615–626). Birkhäuser, Basel.

Drucker, D. C., & Prager, W. (1952). Soil mechanics and plastic analysis or limit design. *Quarterly of applied mathematics*, *10*(2), 157–165.

Duretz, T., May, D. A., Gerya, T., & Tackley, P. (2011). Discretization errors and free surface stabilization in the finite difference and marker-in-cell method for applied geodynamics: A numerical study. *Geochemistry, Geophysics, Geosystems*, *12*(7).

Harlow, F. H., & Welch, J. E. (1965). Numerical calculation of time-dependent viscous incompressible flow of fluid with free surface. *The physics of fluids*, *8*(12), 2182–2189.

Hirth, G., & Kohlstedt, D. (2003). Rheology of the upper mantle and the mantle wedge: A view from the experimentalists. *Geophysical monograph-american geophysical union*, *138*, 83–106.

Kaus, B. J., Mühlhaus, H., & May, D. A. (2010). A stabilization algorithm for geodynamic numerical simulations with a free surface. *Physics of the Earth and Planetary Interiors*, *181*(1-2), 12–20.

Kaus, B. J., Popov, A. A., Baumann, T., Pusok, A., Bauville, A., Fernandez, N., & Collignon, M. (2016). Forward and inverse modelling of lithospheric deformation on geological timescales. In *Proceedings of nic symposium.*

Tirel, C., Brun, J.-P., & Burov, E. (2008). Dynamics and structural development of metamorphic core complexes. *Journal of Geophysical Research: Solid Earth*, *113*(B4).